

Bifunctional Monolayer WSe₂/Graphene Self-Stitching Heterojunction Microreactors for Efficient Overall Water Splitting in Neutral Medium

Chun-Hao Chiang, Yueh-Chiang Yang, Jia-Wei Lin, Yung-Chang Lin, Po-Tuan Chen, Chung-Li Dong, Hung-Min Lin, Kwun Man Chan, Yu-Ting Kao, Kazu Suenaga, Po-Wen Chiu,* and Chun-Wei Chen*



Cite This: *ACS Nano* 2022, 16, 18274–18283



Read Online

ACCESS |

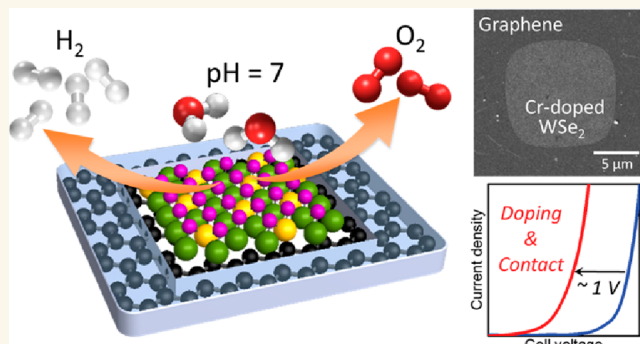
Metrics & More

Article Recommendations

Supporting Information

ABSTRACT: Developing efficient bifunctional electrocatalysts in neutral media to avoid the deterioration of electrodes or catalysts under harsh environments has become the ultimate goal in electrochemical water splitting. This work demonstrates the fabrication of an on-chip bifunctional two-dimensional (2D) monolayer (ML) WSe₂/graphene heterojunction microreactor for efficient overall water splitting in a neutral medium (pH = 7). Through the synergistic atomic growth of the metallic Cr dopant and graphene stitching contact on the 2D ML WSe₂, the bifunctional WSe₂/graphene heterojunction microreactor consisting of a full-cell configuration demonstrates excellent performance for overall water splitting in a neutral medium. Atomic doping of metallic Cr atoms onto the 2D ML WSe₂ effectively facilitates the charge transfer at the solid–liquid interface. In addition, the direct growth of the self-stitching graphene contact with the 2D WSe₂ catalyst largely reduces the contact resistance of the microreactor and further improves the overall water splitting efficiency. A significant reduction of the overpotential of nearly 1000 mV at 10 mA cm⁻² at the Cr-doped WSe₂/graphene heterojunction microreactor compared to the ML pristine WSe₂ counterpart is achieved. The bifunctional WSe₂/graphene self-stitching heterojunction microreactor is an ideal platform to investigate the fundamental mechanism of emerging bifunctional 2D catalysts for overall water splitting in a neutral medium.

KEYWORDS: microreactors, bipolar transport, bifunctional catalysts, neutral water splitting, atomic engineering



INTRODUCTION

Electrochemical water splitting, which includes the hydrogen evolution reaction (HER) and oxygen evolution reaction (OER), is a promising and feasible technology for producing clean hydrogen for sustainable energy conversion.¹ It typically requires voltages larger than the theoretical value of 1.23 V to overcome the activation barriers to initiate the HER and OER decomposition reactions.² The critical challenge of this technique is the search for efficient, low-cost, and long-lasting catalysts that can accelerate the cathodic HER and anodic OER at low overpotentials.³ However, many reported catalysts for the HER and OER usually consist of expensive noble metals such as Pt, Ru, and Ir. The feasibility of scalable industrial applications is largely limited.⁴ Many efforts have been made to develop low-cost electrocatalysts based on earth-abundant elements, such as transition-metal chalcogenides,⁵

phosphides,⁶ oxides,⁷ hydroxides,⁸ alloys,⁹ and doped carbons.¹⁰ These electrocatalysts are usually operated either in a strong acidic solution for the HER or in a strong alkaline solution for the OER to enhance the energy conversion efficiencies by minimizing resistive losses.¹¹ However, these catalysts may suffer from poor activity or stability when the HER and OER electrodes are paired in the same electrolyte for overall water splitting because of an unfavorable pH environment. The construction of bifunctional catalysts that can

Received: June 17, 2022

Accepted: October 25, 2022

Published: October 28, 2022



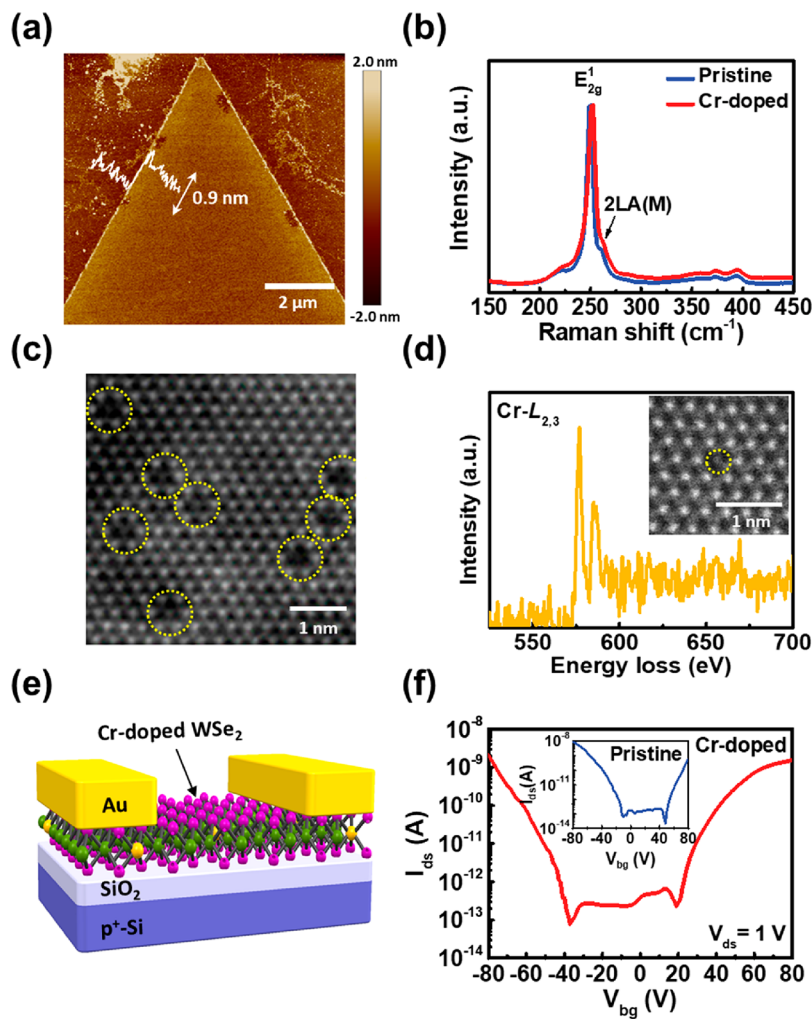


Figure 1. Characterization of the ML CVD-grown Cr-doped WSe₂. (a) AFM image of the as-prepared ML Cr-doped WSe₂ flake on sapphire. (b) Raman spectra of pristine and Cr-doped WSe₂. (c) High-resolution STEM-ADF image of the ML Cr-doped WSe₂. (d) EELS spectrum of the chromium element in the ML Cr-doped WSe₂. (e) Schematic representation of the ML Cr-doped WSe₂ FET device architecture. (f) Room-temperature I_{ds} – V_{bg} characteristics of the pristine (inset) and Cr-doped WSe₂ FET devices.

catalyze both the HER and OER simultaneously in a single electrolyte exhibits great potential in the application of overall water splitting. However, most of the bifunctional catalysts exhibit outstanding HER/OER activities under extreme pH conditions with a strong acid or base, which is corrosive to the electrodes and harmful to the environment.¹² Accordingly, the development of bifunctional electrocatalysts in neutral media to avoid the deterioration of electrodes or catalysts in harsh environments has become the ultimate goal in this field. Several bifunctional catalysts for overall water splitting in neutral media have already been reported, especially transition-metal compounds¹³ such as Ni_{0.1}Co_{0.9}P porous nanosheets¹⁴ and NiS_{2(1-x)}Se_{2x} porous/hollow spheres.¹⁵

Recently, two-dimensional (2D) transition-metal dichalcogenides (TMDs) have emerged as a class of promising ultrathin catalysts for water splitting compared to conventional precious metals. Extensive research has focused on morphology design, doping, defect engineering, and the phase transition of 2D TMDs to enhance their electrocatalytic activities for the HER or OER.¹⁶ The excellent catalytic activity of ultrathin semiconductors such as 2D TMDs is explained by a recently proposed self-gating (or electrolyte-gating) phenomenon where the surface carrier concentrations for 2D

TMD semiconductor catalysts are strongly modulated by electrolyte gating during electrocatalytic reactions.¹⁷ n-type semiconductor catalysts usually favor cathodic reactions, such as the HER, and p-type semiconductor catalysts prefer anodic reactions, such as the OER. For the bifunctional catalysts that can catalyze both the HER and OER simultaneously, bipolar 2D TMD semiconductors that exhibit both n-type and p-type transport behaviors are required. In addition, because of their 2D topography with an atomically thin and flat nature, the monolayer (ML) and few-layer TMD catalysts may work as an ideal platform for exploring the fundamental mechanism of the electrocatalytic reaction.¹⁸ In particular, the utilization of on-chip microcells/microreactors for 2D TMD catalysts demonstrates advantages of directly monitoring the electrocatalytic processes on the surface of individual 2D TMD flakes or films. For example, external field regulation,^{19,20} identification of active sites,²¹ and electronic-conductance modulation¹⁷ on the 2D TMD catalysts can be performed in the on-chip microreactor to monitor their catalytic activities *in situ*. These are difficult to access via conventional electrochemical characterization techniques because these interfaces are generally buried between the solid catalyst and liquid electrolyte.²² Until now, most of the on-chip microreactors

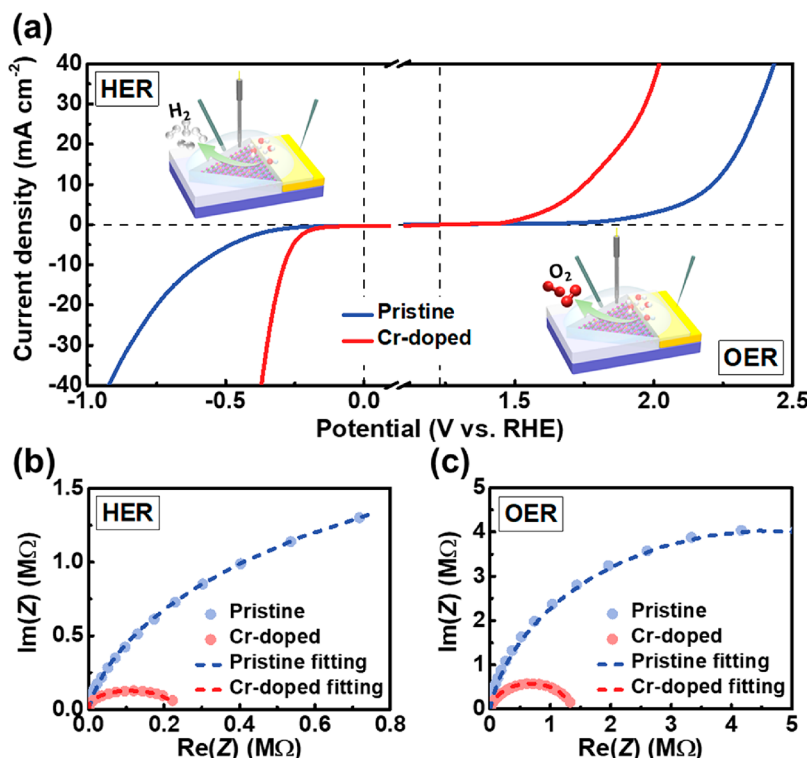


Figure 2. HER and OER catalytic properties of the pristine and Cr-doped WSe_2 microreactors based on the half-cell configuration in a neutral medium. (a) Polarization curves for the HER and OER measured through the half-cell configuration. (b, c) Nyquist plots from the EIS measurement at an overpotential of 600 mV for the HER and OER, respectively.

have been used to investigate the HER or OER reactions of 2D TMD catalysts with a half-cell configuration, where 2D TMD catalysts work as either a cathode or an anode and usually operate only in acidic (or basic) solutions for water splitting.^{23–25} In contrast, an on-chip platform with a full-cell configuration is needed to study the fundamental mechanism of 2D TMD bifunctional catalysts, where 2D TMD bifunctional catalysts play the role of both the anode and cathode for the HER and OER simultaneously.

Among a large number of 2D TMD semiconductors, chemical vapor deposition (CVD) grown ML WSe_2 is a well-known bipolar material that exhibits both n-type and p-type transport behaviors depending on the positive or negative gate polarities.²⁶ This work demonstrates an on-chip bifunctional WSe_2 /graphene heterojunction microreactor for efficient overall water splitting in a neutral medium ($\text{pH} = 7$). Through the synergistic atomic growth of the metallic Cr dopant and graphene stitching contact on the 2D ML WSe_2 , the on-chip bifunctional Cr-doped WSe_2 /graphene heterojunction microreactors with a full-cell configuration demonstrate an excellent performance for overall water splitting in a neutral medium. It is found that atomic doping of metallic Cr atoms onto WSe_2 can effectively facilitate the charge transfer at the solid–liquid interface. In addition, the direct growth of the graphene stitching contact with the 2D WSe_2 catalyst further improves the overall water splitting efficiency of the bifunctional microreactors. A significant reduction of the cell voltage of nearly 1000 mV at 10 mA cm^{-2} at the Cr-doped WSe_2 /graphene heterojunction microreactor compared to the ML pristine WSe_2 microreactor is achieved after performing synergistic atomic engineering on the doping and self-stitching contact. The bifunctional Cr-doped WSe_2 /graphene self-stitching heterojunction on-chip microreactor consisting of a

full-cell configuration is an ideal platform to investigate the fundamental mechanism of emerging bifunctional TMD catalysts for overall water splitting during the electrochemical reaction.

RESULTS AND DISCUSSION

The ML pristine WSe_2 was grown on a c-plane sapphire substrate through the conventional CVD method, as shown in Figure S1. It has been shown that the catalytic activities of 2D TMDs can be largely enhanced by introducing isolated metal atoms to increase the density of active sites and reduce the reaction energy barriers.²⁷ Here, we introduce Cr heteroatoms into the as-grown ML pristine WSe_2 flakes by employing our recently developed two-step postgrowth approach, including postannealing and doping.²⁸ The atomic doping is realized by subliming the Se atoms at the outer surface under the aid of hydrogen and substituting them with Cr heteroatoms at W sites, followed by repairing the lattice. The details of the CVD growth of the ML pristine and Cr-doped WSe_2 flakes are described in the Experimental Section. The optical image of a single Cr-doped WSe_2 flake in Figure S2 shows that a triangular-shaped Cr-doped WSe_2 flake exhibits a lateral size of $\sim 20 \mu\text{m}$. The morphological image obtained by atomic force microscopy (AFM) shown in Figure 1a presents a thickness of $\sim 0.9 \text{ nm}$, indicating a typical signature of the 2D ML flake.²⁹ The Raman spectra of the pristine and Cr-doped WSe_2 are shown in Figure 1b. The Raman feature of the Cr-doped WSe_2 is similar to that of the pristine WSe_2 , indicating that no additional domain is formed after doping.³⁰ The Raman spectrum of Cr-doped WSe_2 displays two characteristic peaks, the E_{2g}^1 mode and the second-order longitudinal acoustic mode 2LA(M) at 250 and 261 cm^{-1} , respectively.³¹ The

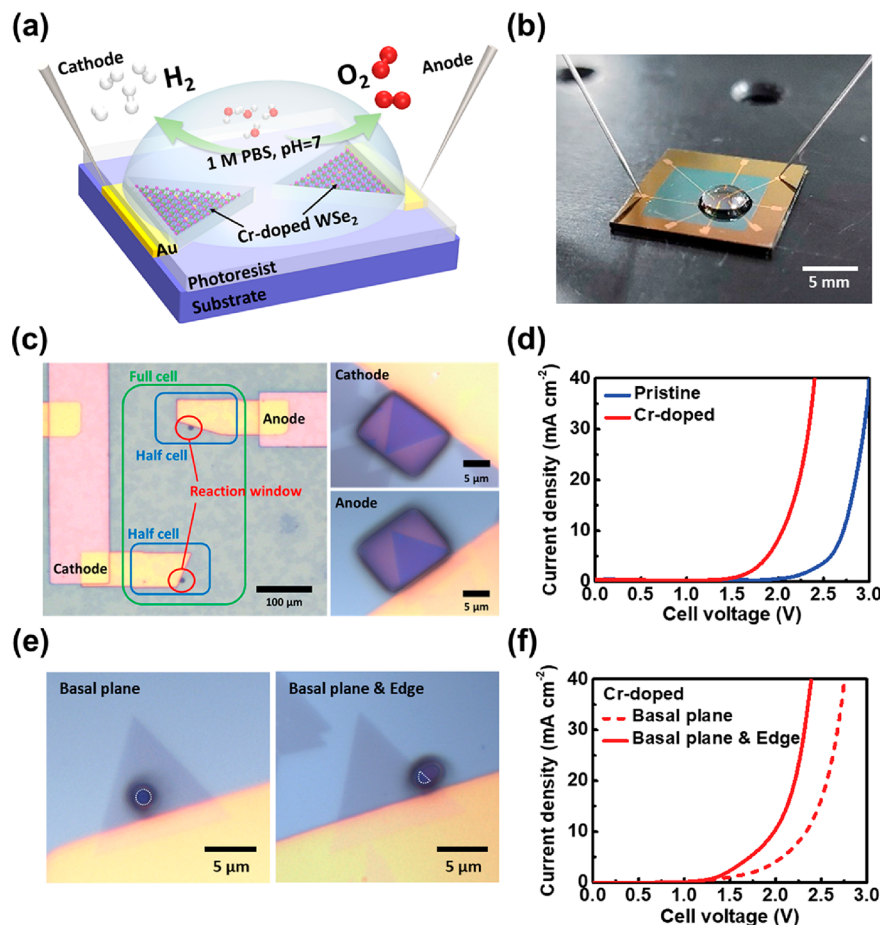


Figure 3. Overall water splitting characteristics in 1 M PBS of the pristine and Cr-doped WSe₂ microreactors based on the full-cell configuration. (a) Schematic illustration and (b) corresponding photograph of the overall water-splitting microreactor. (c) Optical micrograph of the microreactor with reaction windows at the cathode and anode sides. (d) Overall water splitting polarization curves of the pristine and Cr-doped WSe₂. (e) Reaction window with selected area on the basal plane and edge. (f) Overall water splitting polarization curves of the selected areas.

absence of the B_{1g} peak at 308 cm^{-1} , which is related to the interlayer interaction,³² is the typical Raman signature of the ML WSe₂. The atomic structure of the ML Cr-doped WSe₂ was further investigated by atomic-resolution scanning transmission electron microscopy (STEM). Figure 1c shows the annular dark field (ADF) STEM image of Cr-doped WSe₂. Because the Z-contrast intensity of the ADF image strongly depends on the atomic weight, the substitutional dopants of Cr atoms exhibit a reduced contrast in comparison to the W atoms, as marked by the yellow dotted circles. The concentration of Cr dopants is estimated to be $\sim 3.3\%$ in our sample. Although a higher Cr dopant concentration on WSe₂ is possible by our post-treatment approach,²⁸ the appearance of cracks at a higher doping concentration may lead to the discontinuity of the Cr-doped WSe₂ domain, as shown in Figure S4. This may cause the deterioration of the lateral electronic transport, which limits the device performance for the water-splitting application. Figure 1d shows the corresponding spectrum of the monatomic electron energy loss spectroscopy (EELS) from the Cr dopant in the ML Cr-doped WSe₂ flake. Two major features of the Cr-L₂ (586.5 eV) and Cr-L₃ (576.9 eV) peaks can be clearly observed. Other material characterizations such as high-resolution transmission electron microscopy (HRTEM) and X-ray absorption near edge structure (XANES) spectroscopy to support the successful

Cr doping in the ML WSe₂ flake are also provided in the Supporting Information.

As mentioned above, for the bifunctional catalysts that can catalyze both the HER and OER simultaneously, bipolar 2D TMD semiconductors that exhibit both n-type and p-type transport behaviors are required. We also examine the room-temperature electrical properties of the ML Cr-doped WSe₂ by measuring the field-effect transport behavior. The field-effect transistor (FET) device architecture consisting of a global back gate configuration is depicted in Figure 1e. The transfer curve ($I_{ds}-V_{gs}$) of the Cr-doped WSe₂ FET device with a channel width/length of $4/2\text{ }\mu\text{m}$ at a constant $V_{ds} = 1\text{ V}$ is shown in Figure 1f. For comparison, the transport behavior of the ML pristine WSe₂ is also shown (inset of Figure 1f). The transfer curves of both the pristine and Cr-doped WSe₂ FET devices exhibit the bipolar transport behavior with an abrupt increase in I_{ds} as V_{bg} increases for both positive (n-channel) and negative (p-channel) polarities.³³ The symmetric transport behavior with bipolar operation of 2D TMDs is beneficial for their application as bifunctional catalysts for the HER and OER during the overall water splitting reaction.

To examine the electrochemically catalytic activities of the ML Cr-doped WSe₂, we carried out the HER and OER measurements through the microreactor with a half-cell configuration. All of the electrochemical results are presented

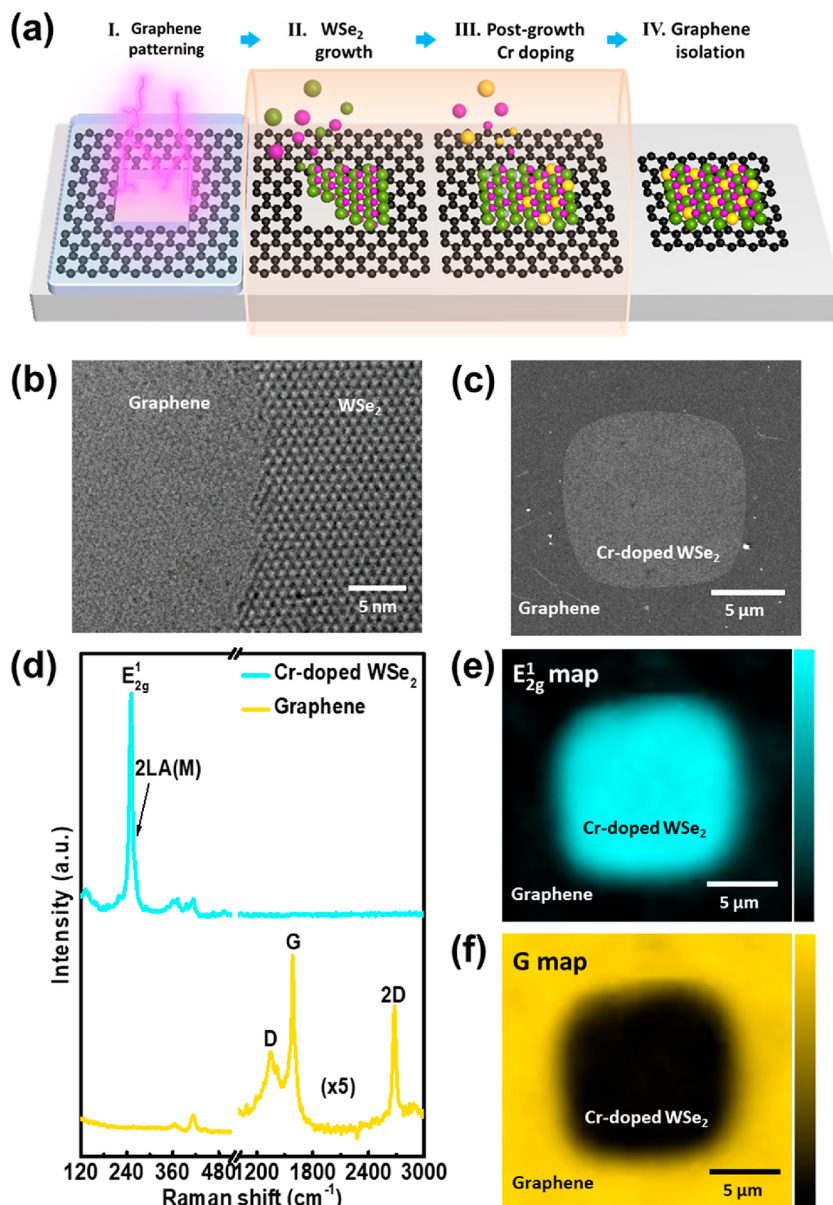


Figure 4. CVD growth procedure and characterization of the Cr-doped WSe₂/graphene heterojunction. (a) Process schematics for the formation of the Cr-doped WSe₂/graphene heterojunction. (b) HRTEM image of the self-stitching contact at the WSe₂/graphene interface. (c) SEM image of the individual Cr-doped WSe₂/graphene heterojunction. (d) Raman spectra of the Cr-doped WSe₂ and graphene domains in (c). (e, f) The corresponding Raman mapping images of the Cr-doped WSe₂ (E_{2g}^1 peak map) and graphene (G peak map) domains.

based on the measurement results of at least ten samples. The standard three-electrode electrochemical measurement system is used to evaluate the performances with Ag/AgCl as the reference electrode, the Pt filament as a counter electrode, and WSe₂ with the gold metal contact as a working electrode. As depicted in the inset of Figure 2a, the ML pristine and Cr-doped WSe₂ were transferred onto the Si/SiO₂ substrates, followed by an optical lithography and thermal evaporation process to pattern the gold contacts and reaction windows. The neutral electrolyte, a droplet of the argon-purged 1 M phosphate buffer solution (PBS) (pH = 7), is placed at the center of the silicon chip. Only the defined reaction windows are exposed to the electrolyte. The cross-linked photoresist covers the rest of the area to avoid undesired current contributions during the measurements. The polarization curves measured by linear sweep voltammetry of the ML

pristine and Cr-doped WSe₂ for the HER and OER are shown in Figure 2a with a scan rate of 5 mV s⁻¹. Here, we define the value of the overpotential when the current density reaches 10 mA cm⁻². The large overpotentials of 600 and 980 mV for the HER and OER are observed for the pristine WSe₂ samples. In contrast, the values of the overpotentials for the Cr-doped WSe₂ are significantly reduced to 290 and 520 mV for the HER and OER, respectively. The corresponding charge transfer resistances at the electrode–electrolyte interfaces for the HER and OER catalytic activities of the pristine and Cr-doped WSe₂ were further analyzed by electrochemical impedance spectroscopy (EIS) measurements, as shown in Figure 2b,c. The semicircle-like Nyquist plot can be fitted by an equivalent circuit consisting of electric-double-layer constant phase elements (Q_{edl}) and charge-transfer resistance (R_{ctr}) in parallel according to the reported model of the

semiconductor catalyst.¹⁷ By fitting the semicircles, the extracted R_{ctr} and Q_{edl} values can be obtained and are shown in Table S1. For both the HER and OER, the R_{ctr} values of the Cr-doped WSe₂ show a decrease from 3.78 to 0.22 MΩ for the HER and from 12.60 to 1.34 MΩ for the OER compared to the pristine WSe₂ as a result of the faster electron shuttling at the electrode–electrolyte interfaces.³⁴ The result indicates that the HER and OER catalytic activities can both be largely enhanced by doping Cr atoms on WSe₂. The promising HER and OER catalytic performances of the ML Cr-doped WSe₂ flakes indicate their great potential as an excellent bifunctional catalyst for overall water splitting. It is noted that all of the data presented here were collected before the possible occurrence of oxidation of the WSe₂ device (<20 cycles). Although the oxidation may also occur in the OER reaction after a long-term operation of the device (>100 cycles), the microreactor device still exhibits excellent bifunctional catalytic performance for overall water splitting due to the superior OER performance of tungsten oxide.³⁵ Details of the performance and stability of the ML pristine and Cr-doped WSe₂ microreactor before and after a long-term operation are provided in the Supporting Information.

Next, as shown schematically in Figure 3a, we fabricated the on-chip overall water-splitting microreactor device by employing two ML Cr-doped WSe₂ electrodes as bifunctional electrocatalysts at both the cathode and anode sides. The corresponding device photograph of the bifunctional on-chip microreactors for overall water splitting is presented in Figure 3b. The aqueous electrolyte droplet (argon-purged 1 M PBS) is dropped at the center of the chip. In contrast to the half-cell microreactor device consisting of three electrodes, the full-cell on-chip microreactor device has two electrodes; one corresponds to the cathode, and the other corresponds to the anode. Figure 3c shows the top view of the full-cell microreactor device, where the cathode and anode are fabricated with a separation distance ($\sim 300 \mu\text{m}$) to prevent the inverted water splitting reactions. Figure 3d shows the corresponding polarization curves of the on-chip microreactors consisting of the ML pristine and Cr-doped WSe₂ bifunctional catalysts. Here, we define the cell voltage of overall water splitting at the voltage applied externally when the current density reaches 10 mA cm⁻². The measured area is defined as the exposed area of the 2D WSe₂ to the electrolyte. The required cell voltage is 2.72 V for the pristine WSe₂ device, while the cell voltage is significantly reduced to 2.05 V for the Cr-doped WSe₂ device. Ascribed to the advantages of on-chip microreactors, we are able to specifically probe the overall water splitting performance of the ML Cr-doped WSe₂ at the basal plane and edge, as seen in Figure 3e. The polarization curves of the on-chip microreactors for overall water splitting at the selected areas are shown in Figure 3f. The cell voltages of the bifunctional Cr-doped WSe₂ microreactors at only the basal plane and the case consisting of both the basal plane and the edge sites are 2.34 and 1.99 V, respectively. The result indicates that the catalytic activity at the edge sites is superior to that in the basal plane. This is consistent with the observation of the outstanding catalytic activities at the edges of 2D TMD semiconductor catalysts analyzed by a half-cell configuration.^{21,36}

In addition to doping, it has also been reported that the role of electrical coupling between the substrate and catalysts to facilitate the injection and collection of charge carriers is crucial for the performance of 2D TMD microreactors.³⁷

Although gold contacts have been widely used as the electrical contacts for 2D TMD microreactors, the deposition of gold directly on top of 2D ML TMD catalysts usually leads to Schottky contacts and the Fermi-level pinning effect, resulting in a high contact resistance.³⁸ Many attempts have been made to solve the issue of the large contact resistance in MoS₂ microreactors for the HER by using the 1T/2H lateral homojunction through phase engineering³⁹ or forming a van der Waals metal contact by vertical stacking heterojunctions.^{40–42} However, the 1T phase of the 2D TMD is thermodynamically unstable and easily transforms into the more stable 2H phase.⁴³ For the vertical heterojunction, the fabrication process of vertically stacking two 2D van der Waals materials at multiple desired positions is quite challenging.⁴⁴ Recently, the direct growth of atomic stitching contact by CVD has been developed to form the lateral graphene/TMD heterojunction.⁴⁵ Previously, we have also demonstrated the nearly pinning free graphene/WSe₂ and graphene/WS₂ junction interfaces for complementary integrated circuits with low contact resistance.³¹ Inspired by this, we combine the atomic doping and stitching contact process to directly grow the bifunctional Cr-doped WSe₂/graphene self-stitching heterojunction microreactors for overall water splitting by fabricating the cathode–anode pairs with well-designed Cr-doped WSe₂/graphene heterojunctions on a single chip. Figure 4a shows the schematic illustration of the Cr-doped WSe₂/graphene self-stitching heterojunction microreactor sequentially formed by the multistep etching and CVD processes. The Cr-doped WSe₂/graphene self-stitching heterojunction microreactor is fabricated on a prepatterned graphene sheet, followed by the growth of the Cr-doped WSe₂ at the specified locations. The detailed deposition processes are described in the Experimental Section. In brief, the oxygen plasma etching process is first performed on a graphene sheet to create the open window (step I). Next, the WSe₂ is only grown on the prepatterned graphene open window in a diffusion-limited mode⁴⁶ (step II), followed by the post-treatment Cr doping process (step III) mentioned earlier. In the final step (step IV), the electrical isolation of graphene is employed to the cathode and anode. It is worth noting that the graphene here not only acts as the contact material but also acts as a template for the growth of the Cr-doped WSe₂. The one-atom-layer graphene can be mildly removed by the bombardment of oxygen plasma. Compared to the van der Waals surface of graphene, the edges of the prepatterned graphene possess substantial dangling bonds after the oxygen plasma treatment during the patterning process.⁴⁷ These dangling bonds can act as nucleation sites for the growth of WSe₂. As we perform the WSe₂ growth in the diffusion-controlled mode, the WSe₂ preferentially grows from the graphene edges and spreads out through the bare sapphire region with the suppressed nucleation of WSe₂ on the clean graphene surface.⁴⁶ Figure 4b shows the image of the self-stitching contact at the WSe₂/graphene interface revealed by HRTEM before the post-treatment Cr doping process. Due to the large lattice mismatch between graphene and WSe₂, direct epitaxial growth from the graphene edge is difficult. Therefore, WSe₂ is overlapped with graphene at the interface to form the stitching contact.³¹

Figure 4c shows the scanning electron microscopy (SEM) image of the individual Cr-doped WSe₂/graphene heterojunction. The Cr-doped WSe₂ at the central part has an area of approximately 12 μm × 12 μm surrounded by the graphene contact. By using Raman spectroscopy, the graphene and Cr-

doped WSe₂ domains with their characteristic peaks can be unambiguously identified. The Raman signatures of both graphene and Cr-doped WSe₂ at the Cr-doped WSe₂/graphene heterojunction are presented in Figure 4d. At the central region of the Cr-doped WSe₂, the Raman peaks of E_{2g}¹ and 2LA(M) positioned at 250 and 261 cm⁻¹, respectively, represent its ML characteristics, as shown above. At the surrounding region of the graphene contact, the typical Raman signatures of the G and 2D peaks located at ~1590 and ~2680 cm⁻¹, respectively, are observed. Except for the G and 2D peaks, there is an intense and broad D peak centered at ~1350 cm⁻¹, which is attributed to the defective sp² carbon, possibly resulting from the conversion of the residual photoresist into amorphous carbon during the CVD growth process at a high temperature.⁴⁷ Figure 4e,f shows the 2D Raman mapping images of the Cr-doped WSe₂/graphene heterojunction with the E_{2g}¹ (251.5 cm⁻¹) peak of Cr-doped WSe₂ and the G (1586.4 cm⁻¹) peak of graphene, respectively. The two distinct domains from the Raman mapping images reveal the macroscopic homogeneity and controllability of the direct growth of Cr-doped WSe₂ onto the prepatterned graphene.

Finally, the electrical isolation of graphene is employed by the second lithography and plasma etching process to separate the cathode and anode pairs to fabricate the bifunctional Cr-doped WSe₂/graphene heterojunction microreactors for the HER and OER in overall water splitting. Figure 5a shows the SEM image of the Cr-doped WSe₂/graphene self-stitching heterojunction pairs after the electrical isolation, which work as cathodes and anodes for overall water splitting. The schematic representation of the Cr-doped WSe₂/graphene heterojunction microreactors for overall water splitting in a neutral medium is shown in Figure 5b. Note that the graphene electrodes are inert with a negligible contribution to water splitting, as seen in Figure S9. The contact resistance value extracted from the graphene/WSe₂ junction is about 1.20 kΩ μm,³¹ which is significantly lower than the values reported for devices with the gold-contact device (~1 MΩ μm).⁴⁸ Accordingly, the Cr-doped WSe₂/graphene heterojunction microreactors exhibit an improved performance with a 310 mV reduction in cell voltage at 10 mA cm⁻² compared to the Cr-doped WSe₂ microreactors with the gold contact, as shown in Figure 5c. Through the synergistic atomic engineering on the doping and stitching contact via post-treatment and direct-growth techniques, the cell voltage of on-chip bifunctional Cr-doped WSe₂/graphene heterojunction microreactors is significantly reduced by 980 mV at 10 mA cm⁻² under a neutral condition compared to that of the pristine WSe₂ microreactors with the conventional gold metal contact. The graphene/TMD self-stitching heterojunction microreactors provide an ideal platform to explore the fundamental mechanisms of electrochemical reactions for emerging 2D catalysts.

CONCLUSION

In summary, we demonstrated the bifunctional Cr-doped WSe₂/graphene self-stitching heterojunction microreactors for overall water splitting in a neutral medium. Due to the bipolar transport behavior, the ML Cr-doped WSe₂ is able to work as a bifunctional electrocatalyst for neutral water splitting based on the full-cell microreactor configuration. The EIS analysis reveals that incorporating Cr heteroatoms into the ML WSe₂ can enhance the charge transfer for both the HER and OER in the neutral medium. Furthermore, relying on the direct-growth CVD process of stitching graphene contact, the Cr-doped

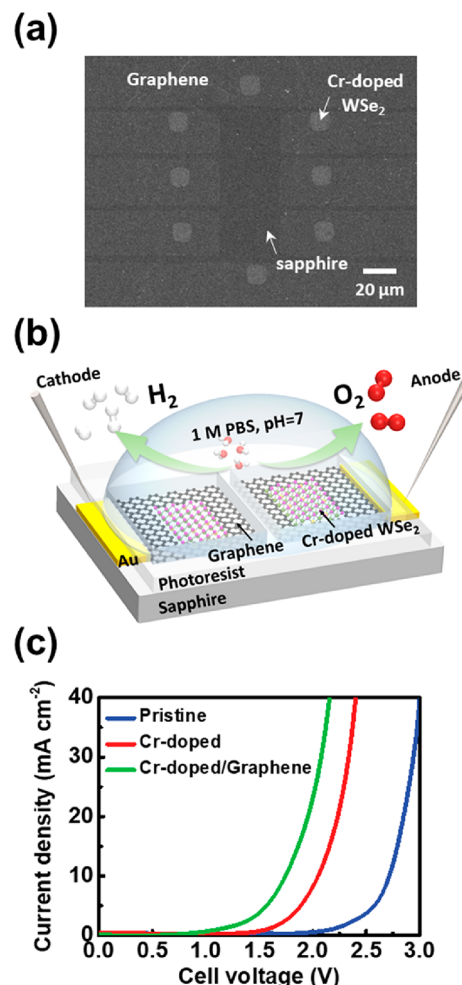


Figure 5. Overall water splitting characteristic in 1 M PBS of the Cr-doped WSe₂/graphene self-stitching heterojunction micro-reactors. (a) SEM image of the electrically isolated Cr-doped WSe₂/graphene heterojunction for cathode and anode pairs. (b) Device schematic of the Cr-doped WSe₂/graphene heterojunction micro-reactors. (c) Polarization curves of the Cr-doped WSe₂/graphene heterojunction micro-reactor and gold contact micro-reactors.

WSe₂/graphene heterojunction microreactor is realized for overall water splitting. Through the synergistic atomic engineering of the Cr doping and the formation of the stitching graphene contact, the Cr-doped WSe₂/graphene heterojunction microreactor exhibits a promising cell performance in neutral overall water splitting compared to that of the pristine WSe₂ microreactor.

EXPERIMENTAL SECTION

Growth of ML Cr-Doped WSe₂. The ML WSe₂ was grown by the CVD method in a quartz tube with high-purity Se (Aldrich, 99.5%) and WO₃ (Alfa Aesar, 99.8%) as precursors and polished sapphire as the growth substrate. The sapphire substrate was cleaned in acetone, isopropyl alcohol, and deionized water with an ultrasonicator before the growth process. The growth process was controlled at a low pressure of 30 Torr with the flow of Ar gas at 120 standard cubic centimeters per minute (scm) and H₂ gas at 30 scm. A typical growth run was performed at 840 °C for 15 min. After the growth, the CVD furnace was cooled to room temperature at a slow rate, and the samples were taken out for the Cr doping process. The Cr source was Cr₂O₃ powder (Alfa Aesar, 99%), which was placed at

the same position as WO_3 in the WSe_2 growth process. The pressure of the doping process was controlled at 20 Torr with the flow of 120 sccm Ar and 10 sccm H_2 . During the doping process, the furnace temperature was set at 720 °C. The first step was H_2 etching for 10 min, which was followed by substitution and lattice repair. Finally, the furnace was also cooled at a slow rate to room temperature.

Growth of the Cr-Doped WSe_2 /Graphene Heterojunction. Graphene was synthesized by atmospheric-pressure CVD onto a 25 μm thick copper foil. The copper foil was cleaned in acetone and isopropyl alcohol and etched in acetic acid at 80 °C for 30 min to remove surface oxides. Prior to the graphene growth, the copper foil was annealed at 1000 °C for over 1 h with a constant flow of 300 sccm Ar and 10 sccm H_2 . For the graphene growth, methane mixed with the 300 sccm Ar and 15 sccm H_2 was fed into the chamber for 1 h. After the growth, the methane flow was stopped, the Ar and H_2 flows were maintained, and the copper foil was moved to the rapid cooling zone. The graphene on the copper foil was transferred onto sapphire using a thin layer of polycarbonate and a HCl aqueous solution. Optical lithography and oxygen plasma etching were performed to pattern the regions for growing the Cr-doped WSe_2 . Then, the growth processes of the Cr-doped WSe_2 were performed to form the Cr-doped WSe_2 /graphene heterojunction.

Characterization of the ML Cr-Doped WSe_2 and Cr-Doped WSe_2 /Graphene Heterojunction. The AFM measurement was performed by using an Olympus OLTESPA tip in tapping mode (Innova, Bruker). STEM and HRTEM images were acquired using a JEOL triple-C#1 microscope, a 2100F microscope equipped with double JEOL delta correctors, and a cold field emission gun operating at 60 kV. The probe current was set 30 pA. For STEM images, the convergence and inner acquisition semiangles are 35 and 79 mrad, respectively. The EELS core loss was recorded by using a Gatan low-voltage quantum spectrometer. Micro-Raman and photoluminescence spectra were collected with a homemade system consisting of an Olympus optical microscope, a large-area scanning stage, a 532 nm continuous-wave laser as the excitation source, an Andor Kymera 193i-B2 spectrometer, and an Andor iDus416 low-noise detector. All of the spectra were acquired with an Olympus 50X objective lens and a power of less than 1 mW. For the FET devices, the WSe_2 was transferred via the conventional PC method onto p-type heavily doped silicon wafers with a 300 nm oxide layer, followed by optical lithography and metal deposition as electrodes. The $I_{ds}-V_{gs}$ curves were measured in the probe station under vacuum. Gate and source-drain voltages were applied by a Keithley 4200A-SCS parameter analyzer and controlled by the program. The SEM measurement was conducted using a Nova NanoSEM 450 instrument.

Fabrication of the Electrochemical Microreactors. For the gold contact sample, the as-grown pristine and Cr-doped WSe_2 were transferred onto a Si/SiO₂ substrate; for the WSe_2 /graphene heterojunction microreactors, the fabrication processes were directly executed on the sapphire substrate without any transfer. The microreactors were fabricated through several optical lithography and thermal evaporation processes to define the metal electrodes on WSe_2 . The reaction windows were patterned through lithography on the target areas. Prior to the electrochemical measurements, all of the devices were annealed in a nitrogen-filled glovebox at 200 °C to harden the photoresist as a strong electrochemically blocking layer.

Electrochemical Measurements of the Microreactors. All of the electrochemical measurements, including the HER, OER, and overall water splitting, were performed by using the Metrohm Autolab PGSTAT204 with the FRA32 M EIS module. For the half-cell configuration, the WSe_2 sample as the working electrode, Pt filament as the counter electrode, and Ag/AgCl as the reference electrode were used. For the full-cell configuration, WSe_2 as both the cathode and anode were probed by tungsten tips, which were manipulated via XYZ micropositioners to apply the potential and collect current. The electrolyte, 1 M PBS, was purged by Ar gas for at least 30 min before use. All of the measurements were performed without iR correction. The polarization curves were measured with a scan rate of 5 mV s⁻¹. The EIS analysis was conducted with a frequency ranging from 10⁶ to 0.01 Hz and an amplitude of 5 mV.

ASSOCIATED CONTENT

Supporting Information

The Supporting Information is available free of charge at <https://pubs.acs.org/doi/10.1021/acsnano.2c05986>.

Additional optical micrographs, photoluminescence spectra, Raman spectra, AFM image, HRTEM image, XANES spectrum, Tafel plots of the HER and OER, EIS analysis result, and water splitting performances of WSe_2 , Cr-doped WSe_2 , and their heterojunctions ([PDF](#))

AUTHOR INFORMATION

Corresponding Authors

Po-Wen Chiu — Department of Electrical Engineering, National Tsing Hua University, Hsinchu 30013, Taiwan; Institute of Atomic and Molecular Sciences, Academia Sinica, Taipei 10617, Taiwan; [orcid.org/0000-0003-4909-0310](#); Email: pwchiu@ee.nthu.edu.tw

Chun-Wei Chen — Department of Materials Science and Engineering, Center for Condensed Matter Sciences, and Center of Atomic Initiative for New Materials (AI-MAT), National Taiwan University, Taipei 10617, Taiwan; [orcid.org/0000-0003-3096-249X](#); Email: chunwei@ntu.edu.tw

Authors

Chun-Hao Chiang — Department of Materials Science and Engineering, National Taiwan University, Taipei 10617, Taiwan; [orcid.org/0000-0002-9066-4657](#)

Yueh-Chiang Yang — Department of Electrical Engineering, National Tsing Hua University, Hsinchu 30013, Taiwan

Jia-Wei Lin — Center for Condensed Matter Sciences, National Taiwan University, Taipei 10617, Taiwan

Yung-Chang Lin — National Institute of Advanced Industrial Science and Technology (AIST), Tsukuba 305-8565, Japan; [orcid.org/0000-0002-3968-7239](#)

Po-Tuan Chen — Department of Vehicle Engineering, National Taipei University of Technology, Taipei 10608, Taiwan

Chung-Li Dong — Department of Physics, Tamkang University, New Taipei City 25137, Taiwan; [orcid.org/0000-0002-4289-4677](#)

Hung-Min Lin — Department of Materials Science and Engineering, National Taiwan University, Taipei 10617, Taiwan

Kwun Man Chan — Department of Materials Science and Engineering, National Taiwan University, Taipei 10617, Taiwan

Yu-Ting Kao — Department of Materials Science and Engineering, National Taiwan University, Taipei 10617, Taiwan

Kazu Suenaga — National Institute of Advanced Industrial Science and Technology (AIST), Tsukuba 305-8565, Japan; The Institute of Scientific and Industrial Research (ISIR-SANKEN), Osaka University, Osaka 567-0047, Japan

Complete contact information is available at:

<https://pubs.acs.org/10.1021/acsnano.2c05986>

Author Contributions

C.-W.C. and P.-W.C. supervised this study. Y.-C.Y. carried out the material growth and preparation. Y.-C.L. and K.S. performed the TEM, STEM, and EELS analyses. C.-H.C. and H.-M.L. fabricated the microreactors and measured the related catalytic performances. C.-H.C., J.-W.L., P.-T.C., C.-

L.D., K.M.C., and Y.-T.K. collected other characterization data. C.-W.C., P.-W.C., and C.-H.C. wrote and revised the manuscript. All authors agreed to the manuscript content.

Notes

The authors declare no competing financial interest.

ACKNOWLEDGMENTS

C.-W.C. acknowledges financial support from the Ministry of Science and Technology (MOST), Taiwan (Grant No. 109-2124-M-002-002-MY3). Financial support by the Center of Atomic Initiative for New Materials (AI-Mat), National Taiwan University, from the Featured Areas Research Center Program within the framework of the Higher Education Sprout Project by the Ministry of Education in Taiwan (Grant No. 108L9008), is also acknowledged. P.-W.C. acknowledges MOST 110-2119-M-007-003-MBK. Y.-C.L. and K.S. acknowledge JSPS-KAKENHI (JP16H06333, 18K14119), the JST-CREST program (JPMJCR20B1, JMJC20B5, JPMJCR1993), and the JSPS A3 Foresight Program. We thank Dr. Hayashi and the Computer and Information Network Center at National Taiwan University for providing calculation resources.

REFERENCES

- (1) Du, J.; Li, F.; Sun, L. Metal-organic frameworks and their derivatives as electrocatalysts for the oxygen evolution reaction. *Chem. Soc. Rev.* **2021**, *50*, 2663–2695.
- (2) Roger, I.; Shipman, M. A.; Symes, M. D. Earth-abundant catalysts for electrochemical and photoelectrochemical water splitting. *Nat. Rev. Chem.* **2017**, *1*, 1–13.
- (3) Wu, T.; Dong, C.; Sun, D.; Huang, F. Enhancing electrocatalytic water splitting by surface defect engineering in two-dimensional electrocatalysts. *Nanoscale* **2021**, *13*, 1581–1595.
- (4) Li, R.-Q.; Hu, P.; Miao, M.; Li, Y.; Jiang, X.-F.; Wu, Q.; Meng, Z.; Hu, Z.; Bando, Y.; Wang, X.-B. CoO-modified Co_3N as a heterostructured electrocatalyst for highly efficient overall water splitting in neutral media. *J. Mater. Chem. A* **2018**, *6*, 24767–24772.
- (5) Zhou, H.; Yu, F.; Huang, Y.; Sun, J.; Zhu, Z.; Nielsen, R. J.; He, R.; Bao, J.; Goddard, W. A., III; Chen, S.; Ren, Z. Efficient hydrogen evolution by ternary molybdenum sulfoselenide particles on self-standing porous nickel diselenide foam. *Nat. Commun.* **2016**, *7*, 12765.
- (6) Xu, J.; Li, J.; Xiong, D.; Zhang, B.; Liu, Y.; Wu, K.-H.; Amorim, I.; Li, W.; Liu, L. Trends in activity for the oxygen evolution reaction on transition metal ($M = \text{Fe}, \text{Co}, \text{Ni}$) phosphide pre-catalysts. *Chem. Sci.* **2018**, *9*, 3470–3476.
- (7) Suryanto, B. H. R.; Wang, Y.; Hocking, R. K.; Adamson, W.; Zhao, C. Overall electrochemical splitting of water at the heterogeneous interface of nickel and iron oxide. *Nat. Commun.* **2019**, *10*, 5599.
- (8) Zhang, X.; Liang, Y. Nickel hydr(oxy)oxide nanoparticles on metallic MoS_2 nanosheets: a synergistic electrocatalyst for hydrogen evolution reaction. *Adv. Sci.* **2018**, *5*, 1700644.
- (9) Jin, Z.; Lv, J.; Jia, H.; Liu, W.; Li, H.; Chen, Z.; Lin, X.; Xie, G.; Liu, X.; Sun, S.; Qiu, H. J. Nanoporous Al-Ni-Co-Ir-Mo high-entropy alloy for record-high water splitting activity in acidic environments. *Small* **2019**, *15*, 1904180.
- (10) Wu, Y.; Tao, X.; Qing, Y.; Xu, H.; Yang, F.; Luo, S.; Tian, C.; Liu, M.; Lu, X. Cr-doped FeNi-P nanoparticles encapsulated into N-doped carbon nanotube as a robust bifunctional catalyst for efficient overall water splitting. *Adv. Mater.* **2019**, *31*, 1900178.
- (11) Naito, T.; Shinagawa, T.; Nishimoto, T.; Takanabe, K. Water electrolysis in saturated phosphate buffer at neutral pH. *ChemSusChem* **2020**, *13*, 5921–5933.
- (12) Li, X.; Hao, X.; Abudula, A.; Guan, G. Nanostructured catalysts for electrochemical water splitting: current state and prospects. *J. Mater. Chem. A* **2016**, *4*, 11973–12000.
- (13) Peng, J.; Dong, W.; Wang, Z.; Meng, Y.; Liu, W.; Song, P.; Liu, Z. Recent advances in 2D transition metal compounds for electrocatalytic full water splitting in neutral media. *Mater. Today Adv.* **2020**, *8*, 100081.
- (14) Wu, R.; Xiao, B.; Gao, Q.; Zheng, Y.-R.; Zheng, X.-S.; Zhu, J.-F.; Gao, M.-R.; Yu, S.-H. A janus nickel cobalt phosphide catalyst for high-efficiency neutral-pH water splitting. *Angew. Chem., Int. Ed.* **2018**, *57*, 15445–15449.
- (15) Zeng, L.; Sun, K.; Chen, Y.; Liu, Z.; Chen, Y.; Pan, Y.; Zhao, R.; Liu, Y.; Liu, C. Neutral-pH overall water splitting catalyzed efficiently by a hollow and porous structured ternary nickel sulfoselenide electrocatalyst. *J. Mater. Chem. A* **2019**, *7*, 16793–16802.
- (16) Chen, Y.; Yang, K.; Jiang, B.; Li, J.; Zeng, M.; Fu, L. Emerging two-dimensional nanomaterials for electrochemical hydrogen evolution. *J. Mater. Chem. A* **2017**, *5*, 8187–8208.
- (17) He, Y.; He, Q.; Wang, L.; Zhu, C.; Golani, P.; Handoko, A. D.; Yu, X.; Gao, C.; Ding, M.; Wang, X.; Liu, F.; Zeng, Q.; Yu, P.; Guo, S.; Yakobson, B. I.; Wang, L.; Seh, Z. W.; Zhang, Z.; Wu, M.; Wang, Q. J.; et al. Self-gating in semiconductor electrocatalysis. *Nat. Mater.* **2019**, *18*, 1098–1104.
- (18) Chia, X.; Pumera, M. Characteristics and performance of two-dimensional materials for electrocatalysis. *Nat. Catal.* **2018**, *1*, 909–921.
- (19) Wang, Y.; Udyavara, S.; Neurock, M.; Frisbie, C. D. Field effect modulation of electrocatalytic hydrogen evolution at back-gated two-dimensional MoS_2 electrodes. *Nano Lett.* **2019**, *19*, 6118–6123.
- (20) Yan, M.; Pan, X.; Wang, P.; Chen, F.; He, L.; Jiang, G.; Wang, J.; Liu, J. Z.; Xu, X.; Liao, X.; Yang, J.; Mai, L. Field-effect tuned adsorption dynamics of VSe_2 nanosheets for enhanced hydrogen evolution reaction. *Nano Lett.* **2017**, *17*, 4109–4115.
- (21) Zhang, J.; Wu, J.; Guo, H.; Chen, W.; Yuan, J.; Martinez, U.; Gupta, G.; Mohite, A.; Ajayan, P. M.; Lou, J. Unveiling active sites for the hydrogen evolution reaction on monolayer MoS_2 . *Adv. Mater.* **2017**, *29*, 1701955.
- (22) Yang, H.; He, Q.; Liu, Y.; Li, H.; Zhang, H.; Zhai, T. On-chip electrocatalytic microdevice: an emerging platform for expanding the insight into electrochemical processes. *Chem. Soc. Rev.* **2020**, *49*, 2916–2936.
- (23) Wang, F.; Shifa, T. A.; Zhan, X.; Huang, Y.; Liu, K.; Cheng, Z.; Jiang, C.; He, J. Recent advances in transition-metal dichalcogenide based nanomaterials for water splitting. *Nanoscale* **2015**, *7*, 19764–19788.
- (24) Pan, X.; Hong, X.; Xu, L.; Li, Y.; Yan, M.; Mai, L. On-chip micro/nano devices for energy conversion and storage. *Nano Today* **2019**, *28*, 100764.
- (25) Zhu, X.; Wang, C.; Fu, L. Engineering electrocatalytic microcells for two-dimensional materials. *Cell Rep. Phys. Sci.* **2020**, *1*, 100190.
- (26) Das, S.; Appenzeller, J. WSe_2 field effect transistors with enhanced ambipolar characteristics. *Appl. Phys. Lett.* **2013**, *103*, 103501.
- (27) Duan, H.; Wang, C.; Li, G.; Tan, H.; Hu, W.; Cai, L.; Liu, W.; Li, N.; Ji, Q.; Wang, Y.; Lu, Y.; Yan, W.; Hu, F.; Zhang, W.; Sun, Z.; Qi, Z.; Song, L.; Wei, S. Single-atom-layer catalysis in a MoS_2 monolayer activated by long-range ferromagnetism for the hydrogen evolution reaction: beyond single-atom catalysis. *Angew. Chem., Int. Ed.* **2021**, *60*, 7251–7258.
- (28) Lin, Y.-C.; Karthikeyan, J.; Chang, Y.-P.; Li, S.; Kretschmer, S.; Komsa, H.-P.; Chiu, P.-W.; Krasheninnikov, A. V.; Suenaga, K. Formation of highly doped nanostripes in 2D transition metal dichalcogenides via a dislocation climb mechanism. *Adv. Mater.* **2021**, *33*, 2007819.
- (29) Zhou, Y.; Zhang, J.; Song, E.; Lin, J.; Zhou, J.; Suenaga, K.; Zhou, W.; Liu, Z.; Liu, J.; Lou, J.; Fan, H. J. Enhanced performance of in-plane transition metal dichalcogenides monolayers by configuring local atomic structures. *Nat. Commun.* **2020**, *11*, 2253.

- (30) Li, S.; Hong, J.; Gao, B.; Lin, Y.-C.; Lim, H. E.; Lu, X.; Wu, J.; Liu, S.; Tateyama, Y.; Sakuma, Y.; Tsukagoshi, K.; Suenaga, K.; Taniguchi, T. Tunable doping of rhenium and vanadium into transition metal dichalcogenides for two-dimensional electronics. *Adv. Sci.* **2021**, *8*, 2004438.
- (31) Yeh, C.-H.; Liang, Z.-Y.; Lin, Y.-C.; Chen, H.-C.; Fan, T.; Ma, C.-H.; Chu, Y.-H.; Suenaga, K.; Chiu, P.-W. Graphene-transition metal dichalcogenide heterojunctions for scalable and low-power complementary integrated circuits. *ACS Nano* **2020**, *14*, 985–992.
- (32) Huang, J.-K.; Pu, J.; Hsu, C.-L.; Chiu, M.-H.; Juang, Z.-Y.; Chang, Y.-H.; Chang, W.-H.; Iwasa, Y.; Takenobu, T.; Li, L.-J. Large-area synthesis of highly crystalline WSe₂ monolayers and device applications. *ACS Nano* **2014**, *8*, 923–930.
- (33) Lin, Y.-F.; Xu, Y.; Wang, S.-T.; Li, S.-L.; Yamamoto, M.; Aparecido-Ferreira, A.; Li, W.; Sun, H.; Nakaharai, S.; Jian, W.-B.; Ueno, K.; Tsukagoshi, K. Ambipolar MoTe₂ transistors and their applications in logic circuits. *Adv. Mater.* **2014**, *26*, 3263–3269.
- (34) Kuraganti, V.; Jain, A.; Bar-Ziv, R.; Ramasubramaniam, A.; Bar-Sadan, M. Manganese doping of MoSe₂ promotes active defect sites for hydrogen evolution. *ACS Appl. Mater. Interfaces* **2019**, *11*, 25155–25162.
- (35) Wondimu, T. H.; Bayeh, A. W.; Kabtamu, D. M.; Xu, Q.; Leung, P.; Shah, A. A. Recent progress on tungsten oxide-based materials for the hydrogen and oxygen evolution reactions. *Int. J. Hydrog. Energy* **2022**, *47*, 20378–20397.
- (36) Kong, D.; Wang, H.; Cha, J. J.; Pasta, M.; Koski, K. J.; Yao, J.; Cui, Y. Synthesis of MoS₂ and MoSe₂ films with vertically aligned layers. *Nano Lett.* **2013**, *13*, 1341–1347.
- (37) Voiry, D.; Fullon, R.; Yang, J.; de Carvalho Castro e Silva, C.; Kappera, R.; Bozkurt, I.; Kaplan, D.; Lagos, M. J.; Batson, P. E.; Gupta, G.; Mohite, A. D.; Dong, L.; Er, D.; Shenoy, V. B.; Asefa, T.; Chhowalla, M. The role of electronic coupling between substrate and 2D MoS₂ nanosheets in electrocatalytic production of hydrogen. *Nat. Mater.* **2016**, *15*, 1003.
- (38) Liu, Y.; Guo, J.; Zhu, E.; Liao, L.; Lee, S.-J.; Ding, M.; Shakir, I.; Gambin, V.; Huang, Y.; Duan, X. Approaching the Schottky-Mott limit in van der Waals metal-semiconductor junctions. *Nature* **2018**, *557*, 696–700.
- (39) Zhang, W.; Liao, X.; Pan, X.; Yan, M.; Li, Y.; Tian, X.; Zhao, Y.; Xu, L.; Mai, L. Superior hydrogen evolution reaction performance in 2H-MoS₂ to that of 1T phase. *Small* **2019**, *15*, 1900964.
- (40) Zhou, Y.; Pondick, J. V.; Silva, J. L.; Woods, J. M.; Hynek, D. J.; Matthews, G.; Shen, X.; Feng, Q.; Liu, W.; Lu, Z.; Liang, Z.; Brena, B.; Cai, Z.; Wu, M.; Jiao, L.; Hu, S.; Wang, H.; Araujo, C. M.; Cha, J. J. Unveiling the interfacial effects for enhanced hydrogen evolution reaction on MoS₂/WTe₂ hybrid structures. *Small* **2019**, *15*, 1900078.
- (41) Liu, X.; Li, B.; Li, X.; Harutyunyan, A. R.; Hone, J.; Esposito, D. V. The critical role of electrolyte gating on the hydrogen evolution performance of monolayer MoS₂. *Nano Lett.* **2019**, *19*, 8118–8124.
- (42) He, Y.; Tang, P.; Hu, Z.; He, Q.; Zhu, C.; Wang, L.; Zeng, Q.; Golani, P.; Gao, G.; Fu, W.; Huang, Z.; Gao, C.; Xia, J.; Wang, X.; Wang, X.; Zhu, C.; Ramasse, Q. M.; Zhang, A.; An, B.; Zhang, Y.; et al. Engineering grain boundaries at the 2D limit for the hydrogen evolution reaction. *Nat. Commun.* **2020**, *11*, 57.
- (43) Lei, Z.; Zhan, J.; Tang, L.; Zhang, Y.; Wang, Y. Recent development of metallic (1T) phase of molybdenum disulfide for energy conversion and storage. *Adv. Energy Mater.* **2018**, *8*, 1703482.
- (44) Gong, Y.; Lin, J.; Wang, X.; Shi, G.; Lei, S.; Lin, Z.; Zou, X.; Ye, G.; Vajtai, R.; Yakobson, B. I.; Terrones, H.; Terrones, M.; Tay, B. K.; Lou, J.; Pantelides, S. T.; Liu, Z.; Zhou, W.; Ajayan, P. M. Vertical and in-plane heterostructures from WS₂/MoS₂ monolayers. *Nat. Mater.* **2014**, *13*, 1135–1142.
- (45) Ling, X.; Lin, Y.; Ma, Q.; Wang, Z.; Song, Y.; Yu, L.; Huang, S.; Fang, W.; Zhang, X.; Hsu, A. L.; Bie, Y.; Lee, Y.-H.; Zhu, Y.; Wu, L.; Li, J.; Jarillo-Herrero, P.; Dresselhaus, M.; Palacios, T.; Kong, J. Parallel stitching of 2D materials. *Adv. Mater.* **2016**, *28*, 2322–2329.
- (46) Yeh, C.-H.; Liang, Z.-Y.; Lin, Y.-C.; Ma, C.-H.; Chu, Y.-H.; Suenaga, K.; Chiu, P.-W. Scalable T-gate aligned Gr–WS₂–Gr radio-frequency field-effect transistors. *ACS Appl. Electron. Mater.* **2020**, *2*, 3898–3905.
- (47) Zheng, C.; Zhang, Q.; Weber, B.; Ilatikhameneh, H.; Chen, F.; Sahasrabudhe, H.; Rahman, R.; Li, S.; Chen, Z.; Hellerstedt, J.; Zhang, Y.; Duan, W. H.; Bao, Q.; Fuhrer, M. S. Direct observation of 2D electrostatics and ohmic contacts in template-grown graphene/WS₂ heterostructures. *ACS Nano* **2017**, *11*, 2785–2793.
- (48) Tosun, M.; Chuang, S.; Fang, H.; Sachid, A. B.; Hettick, M.; Lin, Y.; Zeng, Y.; Javey, A. High-gain inverters based on WSe₂ complementary field-effect transistors. *ACS Nano* **2014**, *8*, 4948–4953.

□ Recommended by ACS

Composite 2D Nanointerfaces for Electrochemical Biosensing: An Experimental and Theoretical Study

Renu Kumari, Penny Poomani Govender, et al.

NOVEMBER 23, 2020

ACS APPLIED BIO MATERIALS

READ ▶

Engineering Phase Stability of Semimetallic MoS₂ Monolayers for Sustainable Electrocatalytic Hydrogen Production

Kunkun Nie, Zhengqing Liu, et al.

APRIL 20, 2022

ACS APPLIED MATERIALS & INTERFACES

READ ▶

Composites of NiS₂ Microblocks, MoS₂ Nanosheets, and Reduced Graphene Oxide for Energy Storage and Electrochemical Detection of Bisphenol A

Jingjing Yuan, Haiqun Chen, et al.

MAY 27, 2021

ACS APPLIED NANO MATERIALS

READ ▶

Scalable In Situ Synthesis of 2D–2D-Type Graphene-Wrapped SnS₂ Nanohybrids for Enhanced Supercapacitor and Electrocatalytic Applications

Sunil. P. Lonkar, Saeed M. Alhassan, et al.

APRIL 07, 2020

ACS APPLIED ENERGY MATERIALS

READ ▶

Get More Suggestions >